Accepted Manuscript

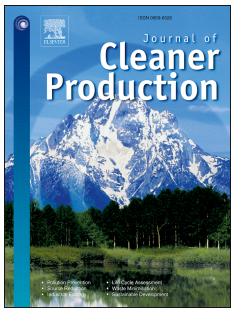

Reduced alkali-silica reaction damage in recycled glass mortar samples with supplementary cementitious materials

Shuaicheng Guo, Qingli Dai, Xiao Sun, Xianghui Xiao, Ruizhe Si, Jiaqing Wang

PII: S0959-6526(17)32792-0

DOI: 10.1016/j.jclepro.2017.11.119

Reference: JCLP 11258

To appear in: *Journal of Cleaner Production*

Received Date: 23 July 2017

Revised Date: 25 September 2017

Accepted Date: 16 November 2017

Please cite this article as: Guo S, Dai Q, Sun X, Xiao X, Si R, Wang J, Reduced alkali-silica reaction damage in recycled glass mortar samples with supplementary cementitious materials, *Journal of Cleaner Production* (2017), doi: 10.1016/j.jclepro.2017.11.119.

Reduced Alkali-Silica Reaction Damage in Recycled Glass Mortar Samples with Supplementary Cementitious Materials

Shuaicheng Guo[1], Qingli Dai[2]*, Xiao Sun[3], Xianghui Xiao[4], Ruizhe Si[5], Jiaqing Wang[6]

Abstract

Recycling waste glass aggregate into concrete can reduce environmental impacts but also may lead to serious alkali silica reaction (ASR) damage. This study aims to characterize ASR damage development in the mortar samples containing reactive glass aggregates and investigate the damage reduction effect of the waste supplementary cementitious materials (SCMs), including recycled glass powders and fly ash. The recycled glass aggregate mortar samples with/without SCMs were prepared in this study. The length change tests were first conducted with the prepared mortar samples based on the ASTM C1260 standard. The results demonstrated the added SCMs can largely decrease early-age ASR expansion rate. The optical microscope and Scanning Electron Microscope (SEM) with Energy Dispersive X-ray Spectroscopy (EDS) were further conducted to characterize the ASR damage in mortar samples and investigate the damage mitigation mechanism with added SCMs. The combined SEM imaging and chemical analysis indicated added SCMs can decrease both the alkali and calcium content of the generated ASR gel. In addition, the ASR damage development inside mortar samples were monitored with dynamic micron X-ray CT (μCT) over a reaction period of 63 hour at the temperature of 80°C. The scanning patterns demonstrated the ASR damage can be easily developed from the area with initial cracks and sharp corners. The images of glass power and fly ash samples showed significantly reduced ASR damage. This study showed that adding of SCMs can largely reduce ASR deterioration and thus facilitate the recycling glass particles into concrete.

Key words: Glass Particle, Fluorescent microscope, Supplementary cementitious materials, X-ray computed tomography, SEM-EDS, ASR damage

[1] Research Assistant, Department of Civil and Environmental Engineering, Michigan Technological University, 1400 Townsend Dr., Houghton, MI 49931-1295, USA. Email: sguo3@mtu.edu.
[2] * Associate Professor, Department of Civil and Environmental Engineering, Michigan Technological University, 1400 Townsend Dr., Houghton, MI 49931-1295 (corresponding author), USA. Email: qingdai@mtu.edu.
[3] Research Assistant, Department of Civil and Environmental Engineering, Michigan Technological University, 1400 Townsend Dr., Houghton, MI 49931-1295, USA. Email: xiaos@mtu.edu.
[4] Beamline Scientist, X-ray Science Division, Advanced Photon Source, Argonne National Laboratory, 9700 South Cass Ave, Argonne, IL 60439, USA. Email: xhxiao@aps.anl.gov.
[5] Research Assistant, Department of Civil and Environmental Engineering, Michigan Technological University, 1400 Townsend Dr., Houghton, MI 49931-1295, USA. Email: ruizhes@mtu.edu.
[6] Research Assistant, Department of Civil and Environmental Engineering, Michigan Technological University, 1400 Townsend Dr., Houghton, MI 49931-1295, USA. Email: jiaqingw@mtu.edu.

1. Introduction

The amount of waste glass materials were quickly accumulated with the rapid social-economic development (Yu et al., 2016). Usually the glass materials can be repeatedly recycled without changing its physical-chemical property. However, the crushed waste glass particles with mixed color cannot be recycled and only be sent to landfill (Shayan and Xu, 2004). The accumulated waste glass can cause heavy burden to achieve the sustainable development. Furthermore, the heavy metals contained in colored glass (Co or Cr (Chen et al., 2006)) can lead to serious water or soil pollution. It is thus important to find additional recycling methods and the application of crushed glass as recycled aggregate (Ling et al., 2013) in concrete production can resolve this issue. The chemical composition of the crush glass aggregate (50% or more silica) is similar to that of the normal aggregate used in concrete (Ling and Poon, 2012a). The low water permeable cement paste can confine the glass aggregate and prevent the possible heavy metal leaching (Ling and Poon, 2014a). However, the active silica content in the added glass aggregate can react with the alkaline pore solution in concrete and thus lead to the alkali silica reaction (ASR) damage (Jin, 1998). Under high humid condition (80% or higher relative humidity (Olafsson, 1986)), the generated ASR gel during the reaction can significantly expand and crack concrete material through water imbibing. The field cases with ASR damage have been reported the area with sufficient moisture, like the Furnas dam in Brazil (Kurtis et al., 1998) and the Mactaquac dam in Canada (Hayman et al., 2010), which is in consistent with the requirement for ASR damage as mentioned above. The durability of the concrete infrastructure can thus be seriously damaged and the confinement effect on heavy metal can be deteriorated by the increased water permeability induced by the ASR damage (Davraz and Gündüz, 2008). It is thus important to identify the ASR damage in cementitious materials containing recycled glass aggregate (Hobbs, 1988) and detect its development to better understand the damage mechanism for possible mitigation methods.

The alkali-silica reactivity of the recycled glass particle has been widely studied to examine its alkali-silica reactivity (Shi and Zheng, 2007). Jin et al. (Jin, 1998) studied the ASR damage features of the glass particles in the cementitious materials with the accelerated mortar bar (ASTM C1260), SEM and Energy Dispersive X-ray Spectroscopy (EDS) tests. The influence of glass particle size on the ASR damage were studied. The existence of pessimism size was confirmed, which can cause the most severe ASR destruction (Jin, 1998) . Further experimental study demonstrated the pessimism size was affected by the aggregate reactivity and gel permeability. Bažant et al. (Bažant and Steffens, 2000) built a representative model (one single spherical glass particle inside the unit cement cell) to study the ASR damage properties in concrete containing glass aggregate. The existence of pessimum size can also be confirmed through the model parametric analysis. Rajabipour et al. (Rajabipour et al., 2010) analyzed influence of the existed

initial defects on the size effect of glass aggregate. The residual cracks inside the larger glass aggregate were found to enhance its alkali reactivity, which can explain that severer ASR damage can more easily occur in the mortar samples with larger size glass aggregate. Maraghechi et al. (Maraghechi et al., 2012) further investigated the influence of residual cracks on the aggregate reactivity. Based on the accelerated mortar bar test, the microcracks thinner than 2.5 μm were found to be innocuous. Shi et al. (Shi, 2009) studied the glass dissolution process and the expansion mechanism of the concrete containing glass aggregate. The soda-lime glass can be dissolved when the pore solution is alkaline enough (pH>12). Particularly due to the high alkali content in glass particles, the alkali content in pore solution is not needed to form the expansive ASR gel. Du et al. (Du and Tan, 2013, Du and Tan, 2014) compared the ASR reactivity of glass aggregate with different colors and sizes. The mortar prepared with clear glass aggregate was found to more expansive than the sample with green and brown glass sand. The green particle in the size range of [1.18, 2.36] mm had the highest alkali silica reactivity. Maraghechi et al. (Maraghechi et al., 2016) analyzed the influence of calcium on the glass aggregate dissolution rate in alkaline solution. The relative dense CSH gel can be form on the glass aggregate surface, which can lower its dissolution rate. Currently, the development mechanism of the ASR damage inside glass aggregate is still not clear enough. The examination technique on the ASR reactivity of glass concrete is still mainly dependent on the ASTM standard methods. New techniques are needed to examine ASR damage thoroughly, dynamically and time-efficiently.

Since the discovery of ASR damage (Stanton, 1940), various methods have been applied to evaluate the ASR damage inside cementitious materials, including expansion rate measurement (ASTM C1260, 2014), microwave examination (Donnell et al., 2013), damage stiffness test (Sanchez et al., 2014), acoustic testing (Saint-Pierre et al., 2007) and etc. These methods above are mainly depend on the expanded volume, changed viscoelastic properties or increased water content induced by the ASR damage, which actually can also be generated by the freeze thaw damage (Neville, 1995) or delayed ettringite formation (Taylor et al., 2001). Hence it is difficult to confirm the existence of ASR damage with these methods along, and the microscope examination (Haha et al., 2007) mostly still needs to be further conducted, including the optical microscope (Peterson et al., 2009) and scanning electron microscope (He et al., 2013). The application of microscope method to detect the ASR damage inside cementitious materials has also been widely conducted. Fernandes et al. (Fernandes et al., 2004) applied the SEM technique to study the morphology of the alkali-silica reaction product obtained from a concrete infrastructure after 50-year service. The initially noncrystalline ASR gel was found to transform into Na-rich crystals after 3 month storage in lab. Peterson (Peterson et al., 2006) analyzed the field ASR gel with the petrographic technique, which was obtained from a concrete structure built in late 1890s. Both the amorphous and

crystalline phases can be detected from the alkali silica reaction products. Bulteel (Bulteel et al., 2004) investigated the mechanism of ASR damage with a prepared concrete subsystem, which was contained of flint aggregate, portlandite and potassium hydroxide (KOH). The damaged flint aggregate was examined with both the optical microscope and SEM techniques. The aggregate porosity was found to increase with the ASR damage and the penetration of alkali content into aggregate can also be detected. Šťastná (Šťastná et al., 2012) investigated the ASR damage features in concrete with combined microscopic techniques (cathodoluminescence, polarizing and electron microscope). Compared to the polarizing and electron microscope, the source materials of the reactive silica can be easily identified with the cathodoluminescence microscope. Çopuroğlu (Çopuroğlu et al., 2009) investigated the alkali reactivity of one type basalt rock with the concrete microbar tests and examine the degradation features with the microscopy examination. The ASR gel formed along the aggregate perimeter and within the aggregate can both be detected with the thin section petrography and SEM. The microscope technique has been proved to be a feasible technique for the ASR damage detection at microscale. However, it is still difficult to monitor the ASR damage development with the microscope technique as the specimen will be destructed during the sample preparation.

Aiming at this problem, the non-destructive X-ray Computed Tomography (CT) technique was introduced to monitor the damage development process dynamically. Wan et al. (Wan and Xue, 2013) applied the in situ X-ray CT technique to analyze the compressive damage in cement paste. Based on the grey scale values of scanning patterns, the connection between the external compressive loading and the internal damage was analyzed quantitatively. Stappen et al. (Van Stappen et al., 2016) investigated the self-healing behavior of concrete materials containing capsules. The breakage of the built-in capsules and the leakage of the self-healing agents can be both detected with the micro CT technique. Currently, the application of X-ray CT technique on ASR damage detection is relative limited. Marinoni et al. (Marinoni et al., 2009) first analyzed the ASR damage in mortar cylinder samples with the X-ray CT technique. The progressive dissolution of aggregate and propagation of microcracks can both be detected with the reconstructed 3D images, which demonstrated the feasibility of X-ray CT technique in ASR damage detection. Marinoni et al. (Marinoni et al., 2015) further studied the ASR damage feature with the synchrotron radiation micro X-ray CT (SR Micro CT). The irregular voids induced by aggregate dissolution and the detachment at the aggregate-cement paste interface can both be detected with the SR micro CT technique. Hernández-Cruz et al. (Hernández-Cruz et al., 2016) studied the features of ASR damage in the fiber reinforced mortar sample with the micro CT technique. The voids filled with generated ASR gel can be detected with the micro CT observation and the added fiber was found to be able to restrain the expansion induced by the ASR damage. Currently, the application of dynamic X-ray

CT technique on cementitious materials containing glass aggregate has not been conducted. In this study, both the microscopy and the micro X-ray CT techniques will be applied to investigate the development of ASR damage in mortar samples prepared with the recycled glass aggregate.

Besides the investigation on mechanism, the mitigation methods on ASR damage had also been conducted for the cementitious materials containing reactive glass aggregate (Ling and Poon, 2014b). Ling (Ling and Poon, 2012b) applied fly ash to control the ASR damage in mortar sample containing glass aggregate and the expansion rate can be efficiently controlled by the added fly ash. The amorphous glassy phase (Bhagath Singh and Subramaniam, 2017) inside fly ash can easily participate into the Pozzolanic reaction and lower the pore solution alkalinity. Furthermore the added SCMs can also enhance the sulfate resistance of concrete based on both the experimental (Nie et al., 2014) and numerical simulation results (Nie et al., 2015), reduce the greenhouse gases emitted during the cement production and generate a greener product (Paris et al., 2016). In addition, the fine glass powder can also serve as supplementary cementitious materials (SCMs) to reduce the ASR damage caused by active glass aggregate (Schwarz et al., 2008). Afshinnia (Afshinnia and Rangaraju, 2015) studied the influence of glass powder fineness on controlling the ASR damage. The finer glass powder (17 μm size) was found to work more efficiently than the relative coarser type (70 μm size). Zheng (Zheng, 2016) studied the mitigation mechanism of the added glass powder on ASR expansion. The aluminum content in pore solution was found to increase with the added glass powder, which can reduce the dissolution rate of the reactive silica. Currently, the application of microscope technique to examine the influence of the added glass powder on ASR damage is relative limited, especially for the optical microscope technique.

This study aims to characterize the ASR damage caused by glass aggregate in cementitious materials and the deterioration reduction effect of the added SCMs. The recycled glass aggregate mortar samples with or without SCMs were prepared for this study. The samples were firstly examined with the accelerated mortar bar tests to evaluate the expansion potential. Then the samples were further examined with both the optical microscope and SEM tests to study the detailed ASR damage features. The dynamic micro X-ray Computed Tomography (μCT) tests were further conducted to dynamically study the ASR damage development. This study can help to understand the ASR damage reduction mechanism of the added SCMs for the further field application.

2. Preparation of mortar samples and expansion tests

2.1 Preparation of Mortar Samples for Length Change Test

The mortar samples containing glass particles were prepared for this study and the detailed mixture design following the ASTM C1260 (ASTM C1260, 2014) can be found in Table 1. The reactive glass aggregate obtained from the Vitro Minerals Co. (Vitro Minerals Company, 2016) was used in this study. The No. 8, No. 16, No. 30, No. 50 and No. 100 size glass aggregates were used for the sample preparation, which account for a mass percentage of 10%, 25%, 25%, 25% and 15% respectively. Particularly the color of the waste aggregate used this study were mixed, including white, green, brown and etc. The main contents of glass particle are SiO_2, Al_2O_3, CaO, and Na_2O+K_2O, accounting for a mass percentage of 75±5%, 3±2%, 11±2%, 13±3% respectively (Vitro Minerals Company, 2016). Mortar samples were casted with the Larfage Type 1 cement. The main chemical compositions of the cement are CaO, SiO_2, Al_2O_3 and Fe_2O_3, which account for a mass percentage of 62.8%, 19.4%, 4.9% and 2.8% respectively based on the XRF measurement (Guo et al., 2017). The glass powder and the fly ash was also added into the mortar sample as SCMs to examine the potential on controlling the ASR damage. Totally seven type samples with different SCMs or replacement ratios were prepared as shown in Table 1.

The detailed chemical composition and fineness of the added SCMs are demonstrated in Table 2. The alkali content of the LA type glass powder is similar to that of the CS type and the LA type glass powder has higher alumina content compared to the CS type. The CS325 type glass powder is slightly finer than that of the LA300 type and the particle size of LA800 type glass powder is much smaller than the other two type glass powder. The fly ash has the highest alumina content but the coarsest particle size.

The 2.54 cm by 2.54 cm by 28.575 cm (1 in by 1 in by 11.25 in) mortar bars were prepared based on the ASTM C490 (ASTM International, 2011) for the length change tests. After demolded at 24 hours, the sample initial length was first measured. After the measurement, the samples were submerged into the 80^{o}C water and the zero readings was taken after 24 hour period. After that, the samples were stored into NaOH solution (80 ^{o}C, 1 mol/L) to accelerate the development of ASR damage. The subsequent length change measurement were conducted at 1 day, 3 day, 5 day, 7 day, 14 day, 21 day and 28 day storage age.

2.2 Expansion test and length change analysis

The expansion potential of prepared mortar samples was examined with the accelerated mortar bar tests recommended by ASTM C1260 standard. The measured expansion rate up to 14 day reaction age of the first five type samples shown in Table 1 are demonstrated in Fig.1 a). The expansion rate of the Type 1 sample reached 0.523% at 14 day age, which was much higher than the expansion limit (0.1% at 14 day age) and demonstrated the high alkali reactivity of the glass aggregate. Compared to the type 1 sample, the expansion rate of the Type 2, 3, 4 and 5 samples decrease by 46.6%, 58.1%, 64.9% and 59.30% respectively, which demonstrated the added SCMs can obviously reduce the ASR damage. As the particle

size of the LA300 is very similar to that of the CS325, the improvement on controlling ASR damage can be generated by the relative higher alumina content (Shi and Zheng, 2007). This result indicated the LA type glass powder can control the ASR damage more efficiently. The expansion rate of the type 4 sample was lowest among the five type samples, which indicated the finer glass powder can work more efficiently in reducing the ASR damage (Zeidan and Said, 2017). This finding was in accordance with the results shown in the reference (Afshinnia and Rangaraju, 2015).

Further tests with higher replacement ratio (30%) was conducted for LA300 (Type 6) and LA800 (Type 7) types glass powder as shown in Fig. 1 b). The expansion rate at 28 day age for the type 6 and 7 samples were 0.067% and 0.022% respectively, which were both lower than 0.1%. The results demonstrated the added glass powder can efficiently reduce the ASR damage with sufficient replacement ratio at early stage. The sample containing fly ash has similar reduction effect as the mortar samples with LA type glass powders.

3. Microscope characterization of ASR tested mortar samples

3.1 Surface Polishing and Treatment for the microscope examination

After the length change tests, the samples were further examined with the optical microscope and SEM tests. The mortar bars were firstly surface sawn with a diamond saw cooled with kerosene. The cut samples were further detailed polished for the further examination. To better identify the cracks induced by ASR damage, the samples were dyed with fluorescent epoxy as shown in Figure 1. The sample dyeing process was conducted based on the procedure introduced in the reference (Hanson et al., 2003) with the IU30 Vacuum Impregnation as shown in Fig. 1 a). After dyeing with florescent epoxy, the mortar samples were stored overnight for the epoxy curing as shown in Fig. 1 b).

3.2 The examination of the mitigation effect with microscope method

For optical microscope characterization, the tested samples were surface sawn, polished and dyed with fluorescent epoxy. The examination results of the type 1 sample are shown in Fig.3, where the cracks induced by the ASR damage can be clearly identified with the fluorescent light. The phases with brighter color indicated the developed ASR damage in mortar samples. The ASR damage can lead to obvious cracks inside the glass aggregate as shown in both Fig.3 a) and b). The aggregate-cement paste interface can also be deteriorated by the alkali silica reaction and the cracks along the aggregate perimeter can be detected in both Fig.3 b) and e). The development of ASR damage along the aggregate boundary can lead to the detachment between glass aggregate and cement paste as shown in Fig.3 b). The cracks induced by the expansive gel can propagate from damaged aggregate to surrounding air voids as shown in Fig.3 c)

and f), which can serve as the transport path for alkaline solution and promote the alkali silica reaction. Particularly the sample will be oven dried during the preparation process and the corresponding desiccation cracks can be found on the gel surface as shown in Fig.3 b), which is in accordance with the report in reference (Hanson et al., 2003).

The type 2, 3, 4 and 5 samples were also examined with the microscope technique to examine the reducing effect of the added SCMs on ASR damage. Compared to the Type 1 sample, relatively limited ASR damage can be detected in sample 2, 3, 4 and 5 as shown in Fig.4 a), b) and c) and d) respectively. The almost undamaged aggregate can be found in the areas close to air void as demonstrated in Fig.4, where the ASR damage can easily develop. However, the existence of expansive ASR gel can still be detected inside the sample Type 2, 3, 4 and 5 as shown in Figure 5 a), b), c) and d) respectively. The Fig. 5 a), b) c) and d) indicates the developed damage in glass aggregate, propagated cracks inside glass particle, damaged aggregate besides air voids and the damage developed around the aggregate-cement paste interface respectively. It is also clear that the ASR damage in the samples with added SCMs can be mainly found inside the glass aggregate and the propagated cracks inside cement paste is still very limited. The expansion rate of Type 2, 3, 4 and 5 samples still exceeded the 0.1% limit at 14 day age and the replacement ratio of 15% was not sufficient.

4. Damage characterization and chemical composition analysis with SEM-EDS technique

The ASR features inside mortar samples were further investigated with the Environmental Scanning Electron Microscope (ESEM). The high-resolution cracks can be found inside both aggregate and cement paste. In addition, the EDS with element mapping were also conducted to identify the phase chemical composition.

4.1 ESEM/EDS characterization of control mortar sample

The examination results of the control mortar samples were demonstrated in Fig.6. It is obvious severe ASR damage can be detected in Fig. 6 a), where the whole glass particle has been broken into small parts by the cracks caused by the expansion of ASR gel. It is also clear the ASR damage mainly happen inside the reactive glass aggregate instead of the glass-cement paste interface, which is in accordance with the results in the reference (Rajabipour et al., 2010). The magnification of the Area A shown in Fig. 6 a) is demonstrated in Fig. 6 b), where the cracks developed from the damaged aggregate to surrounding cement paste can be clearly indicated. To better understand the property of the expansive ASR gel and its correlation to the gel composition, the chemical content analysis based on the EDS technique was conducted on the selected sites shown in Fig. 6 b). The chemical composition analysis results of the three

sites shown in Fig. 6 b) were indicated in Table 3, where the gel located in S1, S2 and S3 belonged to the gel inside damaged aggregate, gel along the aggregate-cement interface and gel penetrated to the surrounding cement paste. Particularly, the gel (S3) inside the cracks in cement paste has both high alkali and calcium content as shown in Table 1, which is in accordance with the results that both alkali and calcium contents were needed to generate destructive ASR gel (Vayghan et al., 2016).

The phase analysis in ASR damaged mortar samples shown in Fig.6 b) was furhter conducted based on the element mapping analysis as shown in Fig.6 c), where red, yellow, blue and white colors indicated the concentration of silica, calcium, sodium and aluminum respectively. Particulary, the brighter color indicated higher element concentration. Three different phases can be clearly detected from the element mapping resutls, the unreacted aggregate, the surrounding cement paste and the genereated ASR gel. The silica content in unreacted glass aggregate was highest, followed by the generated ASR gel and the cement paste as depicted in Fig.6 c). The cement paste area had the highest calcium concentration and the calcium content of the generated ASR gel was higher than that of the unreacted aggregate. The gel peneration through the cracks in cement paste can also be obviously detected as shown in Fig.6 c).

4.2 ESEM/EDS characterization of mortar sample with glass powders

The mortars sample with added glass powder (Type 3 and 4) samples were also examined with the ESEM technique to study the corresponding ASR damage features. The examination results of the type 3 and 4 sample are demonstrated in Fig. 7 and Fig. 8 separately. As shown in Fig. 7 a) and Fig. 8 a), the observed cracks can be mainly found inside glass aggregate and the cracks in cement paste are relative limited. The damage level in these two type samples was obviously less severe than the Type 1 sample, which is in accordance with the optical microscope and expansion rate results. The magnification of the selected areas shown in Fig. 7 a) and Fig. 8 a) are indicated in Fig. 7 b) and Fig. 8 b) respectively. The morphology of the ASR gel inside glass aggregate and along the aggregate-cement paste interface can be both observed in Fig. 7 b). The crack tip of the fracture induced by ASR damage can be observed in Fig. 8 b).

The chemical composition analysis of the samples with added glass powder was also conducted. The samples containing LA 300 type glass powder (Type 3 sample) and LA 800 type glass powder (Type 4 sample) were investigated with the EDS tests and the examination sites were indicated in Fig. 7 a) and Fig. 8 a) respectively. The corresponding measurement results were shown in Table 5 and 6 separately. The S1 and S2 shown in Fig. 7 a) belonged to the gel along the aggregate-cement paste interface. The S1 indicated in Fig. 8 a) was the internal gel inside the damaged aggregate, and S2 and S3 indicated the gel along the aggregate-cement paste interface. As shown in Table 4 and 5, the Alkali: Si ratios of the

samples with added glass powder were in similar range compared to the Type 1 sample without added glass powder. However, the calcium content of the ASR gel in samples with glass powder was much lower, which is in agreement with the finding that the added glass powder can lower the calcium content in pore solution (Zheng, 2016).

The sample with added fly ash (Type 5) was further examined with SEM technique to analyze its damage features and the examination results are shown in Fig. 9. The ASR induced damages are mainly limited inside the glass aggregate as shown in Fig. 9 and the surrounding cement paste has not been obviously cracked. The chemical composition analysis based on EDS test was also conducted on the sites shown in Fig. 9 a) and the corresponding results are shown in Table 6. Compared to the samples with glass powder, the sample containing fly ash has a similar Ca:Si ratio but a much lower Alkali:Si ratio. Furthermore, the alumina content of the fly ash sample is obviously higher than both the control sample and the glass powder samples. These results demonstrate the added fly ash can better bind the alkali content and the enhanced binding effect was probably generated from the higher alumina content (Chappex and Scrivener, 2012).

5. The detection of ASR damage using dynamic micro X-ray Computed Tomography (μCT) technique

5.1. The sample preparation and basic setup of micro X-ray CT test

The dynamic μCT tests were conducted at Beamline 2-BM of the Advance Photon Source (APS) at Argonne National Lab. The experiment setup parameters were determined based on the former study on the interaction between glass particle and sodium hydroxide solution (Sun et al., 2017). The scanning resolution was 1 μm/pixel with the selected beam energy (27.4 keV) and exposure time (300 ms). The scanning was proceeded from 0^o to 180^o on each cross section with 1° angular increment. The distance between each cross section is 1 μm.

The preparation of the dynamically scanned sample was conducted based on method used in reference (Guo et al., 2017). The micro scale mortar sample was prepared with the Lafarge Type 1 cement and the recycled glass aggregate from Vitro Minerals (Vitro Minerals Company, 2016). The volume ratio of cement to aggregate and the water/cement ratio in this study were chosen as 0.3 and 0.5 respectively. In addition, the cement was directly mixed with 1 mol/L NaOH solution to promote the ASR development for time-efficient evaluation. The prepared fresh mortar sample was put into a PTFE tube (2 mm inner diameter) and seated with epoxy for the X-ray CT test. To accelerate the reaction, the sample was located at 80 ^oC condition in an furnace as recommended by ASTM C1260 (ASTM C1260, 2014).

Besides the dynamic examination, the static scanning on the pre-prepared samples was also conducted. Three type glass aggregate mortar samples with different SCMs type and content were prepared: the control sample without SCMs, the sample with 30% cement replaced by fly ash and the sample with 30% replaced LA800 type glass powder. The statically scanned samples were prepared with the same glass aggregate used for the dynamically examined samples. The cement was directly mixed with water at 0.47 w/c ratio and the prepared samples were submersed into 80^{o}C water for 24 hours at one day age based on ASTM C1260 (ASTM C1260, 2014). After that the samples were further submersed into 1 mol/L NaOH solution at 80^{o}C for another 7 day age before the μCT examination.

5.2. Experimental image analysis for damage detection

The dynamic μCT scan was conducted with the prepared microscale mortar sample up to 63 hours reaction age. To better demonstrate the development of ASR damage with higher resolution, the scanning results at 0, 12, 36 and 63 reaction hours are demonstrated in Fig. 9 a), b), c) and d) respectively. These figures showed that most of ASR damage or cracks initiated from area with initial defects. These defects were generated during glass particle recycling process. The defects in glass particles can further lead to stress concentration and the fracture can more easily initiate and propagate (Anderson and Anderson, 2005).

The influence of the initial defects on ASR damage development can be more detailed demonstrated by comparing Fig.10 a) and b), which are scanned at initial and final stages (63 hrs) respectively. The Area A shown in Fig. 10 a) was almost intact at the beginning while several initial defects can be found in the Area B. After 63 hours reaction, it is clear the glass aggregate in Area B were more severe damaged compared to Area A as demonstrated in Fig.10 b). These findings further support that the ASR damage can more easily occur in the area with initial defects. By comparing Fig.10 c) and d), the developed radical cracks from the initial defects can be observed. This result indicated the cracks caused by ASR damage can propagate randomly from the initial defects.

In addition to the damage in glass aggregate, the expansive ASR gel can also affect the cement-aggregate bonding. A clear cement-aggregate gap can be found in Area B as demonstrated in Fig.11 b). This phenomenon was in accordance with the findings in the reference (Hernández-Cruz et al., 2016), which is due to the expansion of the generated ASR gel. The damage developed from sharp corner area is indicated in Fig.12, where the cracks were formed from the intact corner area after 63 hours reaction. The cracks can serve as the transport path for alkali ion, which can increase the water permeability of the cementitious materials and promote the development of ASR damage. The dynamic scanning results demonstrate the cracks can more easily develop from the area with initial defects or the sharp corner area.

The expansion of the ASR gel in these area can easily lead to stress concentration (Maraghechi et al., 2012). Furthermore the propagated cracks inside silica materials can lead the strained Si-O-Si bonds (Munekuni et al., 1991) and break the Si-O covalent bonds (Radtsig, 1995). These two defects can significantly enhance the surface reactivity of silica materials (Pacchioni, 2000). The stress concentration and the enhanced reactivity due to structure defects were the two main reasons that the ASR damage in glass aggregate mainly develop from the area with initial defects instead of the glass-cement paste area.

The static μCT scanning results of the pre-prepared samples are shown in Fig.13. The large-amount of ASR induced cracks can be observed with the control sample (without added SCMs) as shown in Fig. 13 a) and d). The ASR damages in the samples with added fly ash and glass powder are both significantly reduced as demonstrated in Fig. 13 b)+e) and c)+f) respectively. The static scanning results further demonstrate the damage reduction effect of the added SCMs.

5. Conclusions

This study demonstrated that the utilizing the waste SCMs into recycled glass particle cement paste can reduce many ASR damage and thus reduce environmental impacts. The ASR damage mechanism in cementitious materials containing glass aggregate were characterized and the damage reduction effects with waste materials (fly ash and glass powder) were also evaluated. The accelerated mortar bar tests were firstly conducted to evaluate expansion. Then the tested samples were further examined with both the optical microscope and SEM tests to investigate the morphology of the ASR damage. The chemical composition of the reaction product was also studied with the EDS technique. The dynamic μCT tests were further conducted to study the ASR damage development in the mortar samples containing glass aggregate. The main conclusions of this paper are listed below.

(1) Both the added fly ash and the glass powder can obviously control the ASR damage during early age in the mortar samples containing reactive glass aggregate. The expansion rate at 14-day age can decrease by 46.6%, 58.1%, 64.9% and 59.30% with 15% replacement ratio of CS325, LA300, LA800 type glass powder and fly ash respectively. The expansion rates were 0.067% and 0.022% for the mortar samples with 30% replacement ratio of LA300 and LA800 type glass powder at 28 day age. Compared to LA300, the LA800 glass powder can work more efficiently in controlling ASR damage due to its finer particle size. Particularly, the reduction effect of the fine glass powder is comparable to that of the fly ash.

(2) The microscope examination results on control samples demonstrate the crack induced by the ASR damage can penetrate from the reactive aggregates to the surrounding cement pastes or air voids, which can increase permeability and reduce durability. The examination on the sample with added SCMs

demonstrate the damage are mainly limited in the glass aggregate and only few cracks in cement paste can be observed, which demonstrate the added SCMs can prevent the increase of water permeability. The examination also indicated ASR damage mainly developed inside the glass aggregate instead of the glass-cement interface. The detachment between the glass aggregate and cement paste induced by the ASR gel expansion can be observed from both optical microscope and SEM tests.

(3) Based on the element mapping analysis, the three main phases (unreacted aggregate, cement paste and ASR gel) in the ASR damaged mortar samples can be clearly identified. The unreacted glass aggregate and cement paste have the highest silica content and calcium concentration respectively. The calcium content of the generated ASR gel is higher than that of the unreacted aggregate. The expansion of the ASR gel into cement paste through the cracks can be clearly detected with the mapping analysis results. The gel inside the cracks in cement paste has both relative high calcium and alkali content, which demonstrate both calcium and alkali content are needed to generate destructive ASR gel. The chemical composition analysis results demonstrate the added SCMs can lower both the alkali and calcium content in the generated ASR gel, which can lead to less expansive and destructive gel.

(4) This X-ray CT scanning results in this study first time provide the direct evidence that the ASR damage can more easily generate from the area with initial defects or sharp corner area. The ASR damage evolution in different scenarios can be observed from the X-ray CT examination, including the development of the radical cracks and the detachment between aggregate and cement paste. Furthermore, the μCT images of glass power and fly ash samples showed significantly reduced ASR damage.

This study examined the damage reduction effect of the waste SCMs in the cementitious materials containing glass aggregates. The current study demonstrated the glass mortar samples had sufficient ASR damage resistance with 30% cement replaced by SCMs, which can applied for further concrete study. Besides mitigating the environmental pressure and reducing the generated CO_2 during cement production, the examination results further demonstrate replacing part of cement with waste glass powder/fly ash can facilitate the waste glass particles into concrete and lead to a both greener and durable building material.

ACKNOWLEDGEMENT

The authors would like to acknowledge the Michigan Department of Environmental Quality for financial support. The authors also like to acknowledge the help on proceeding the X-ray CT tests from Advanced Photon Source at Argonne National Laboratory. The first author acknowledges the financial support from the China Scholarship Council under No. 201406370141 and the Doctoral Finishing Fellowship from the Graduate School of Michigan Technological University.

405

406 Afshinnia, K. and Rangaraju, P. R. (2015). Influence of fineness of ground recycled glass on mitigation of
407 alkali–silica reaction in mortars. Construction and Building Materials **81**: 257-267.
408 Anderson, T. L. and Anderson, T. (2005). Fracture mechanics: fundamentals and applications. CRC press.
409 ASTM C1260 (2014). Standard Test Method for Potential Alkali Reactivity of Aggregates (Mortar-Bar
410 Method), ASTM International, West Conshohocken, PA, 2014, www.astm.org.
411 ASTM International (2011). ASTM C490 / C490M-11e1, Standard Practice for Use of Apparatus for the
412 Determination of Length Change of Hardened Cement Paste, Mortar, and Concrete, West
413 Conshohocken, PA.
414 Bažant, Z. P. and Steffens, A. (2000). Mathematical model for kinetics of alkali–silica reaction in
415 concrete. Cement and Concrete Research **30**(3): 419-428.
416 Bhagath Singh, G. and Subramaniam, K. V. (2017). Direct decomposition X-ray diffraction method for
417 amorphous phase quantification and glassy phase determination in binary blends of siliceous fly ash and
418 hydrated cement. Journal of Sustainable Cement-Based Materials **6**(2): 111-125.
419 Bulteel, D., Rafaï, N., Degrugilliers, P. and Garcia-Diaz, E. (2004). Petrography study on altered flint
420 aggregate by alkali–silica reaction. Materials Characterization **53**(2): 141-154.
421 Chappex, T. and Scrivener, K. L. (2012). The influence of aluminium on the dissolution of amorphous
422 silica and its relation to alkali silica reaction. Cement and Concrete Research **42**(12): 1645-1649.
423 Chen, D., Masui, H., Miyoshi, H., Akai, T. and Yazawa, T. (2006). Extraction of heavy metal ions from
424 waste colored glass through phase separation. Waste management **26**(9): 1017-1023.
425 Çopuroğlu, O., Andiç-Çakir, Ö., Broekmans, M. A. and Kühnel, R. (2009). Mineralogy, geochemistry and
426 expansion testing of an alkali-reactive basalt from western Anatolia, Turkey. Materials Characterization
427 **60**(7): 756-766.
428 Davraz, M. and Gündüz, L. (2008). Reduction of alkali silica reaction risk in concrete by natural
429 (micronised) amorphous silica. Construction and Building Materials **22**(6): 1093-1099.
430 Donnell, K., Zoughi, R. and Kurtis, K. (2013). Demonstration of microwave method for detection of
431 alkali–silica reaction (ASR) gel in cement-based materials. Cement and Concrete Research **44**: 1-7.
432 Du, H. and Tan, K. H. (2013). Use of waste glass as sand in mortar: Part II–Alkali–silica reaction and
433 mitigation methods. Cement and Concrete Composites **35**(1): 118-126.
434 Du, H. and Tan, K. H. (2014). Effect of particle size on alkali–silica reaction in recycled glass mortars.
435 Construction and Building Materials **66**: 275-285.
436 Fernandes, I., Noronha, F. and Teles, M. (2004). Microscopic analysis of alkali–aggregate reaction
437 products in a 50-year-old concrete. Materials Characterization **53**(2): 295-306.
438 Guo, S., Dai, Q., Sun, X. and Xiao, X. (2017). X-Ray CT Characterization and Fracture Simulation of ASR
439 Damage of Glass Particles in Alkaline Solution and Mortar. Theoretical and Applied Fracture Mechanics.
440 Haha, M. B., Gallucci, E., Guidoum, A. and Scrivener, K. L. (2007). Relation of expansion due to alkali
441 silica reaction to the degree of reaction measured by SEM image analysis. Cement and Concrete
442 Research **37**(8): 1206-1214.
443 Hanson, K., Van Dam, T., Peterson, K. and Sutter, L. (2003). Effect of sample preparation on chemical
444 composition and morphology of alkali-silica reaction products. Transportation Research Record: Journal
445 of the Transportation Research Board(1834): 1-7.
446 Hayman, S., Thomas, M., Beaman, N. and Gilks, P. (2010). Selection of an effective ASR-prevention
447 strategy for use with a highly reactive aggregate for the reconstruction of concrete structures at
448 Mactaquac generating station. Cement and Concrete Research **40**(4): 605-610.
449 He, J., Jie, Y., Zhang, J., Yu, Y. and Zhang, G. (2013). Synthesis and characterization of red mud and rice
450 husk ash-based geopolymer composites. Cement and Concrete Composites **37**: 108-118.
451 Hernández-Cruz, D., Hargis, C. W., Dominowski, J., Radler, M. J. and Monteiro, P. J. (2016). Fiber
452 reinforced mortar affected by alkali-silica reaction: A study by synchrotron microtomography. Cement
453 and Concrete Composites **68**: 123-130.

Hobbs, D. W. (1988). Alkali-silica reaction in concrete. Thomas Telford Publishing.
Jin, W. (1998). Alkali-silica reaction in concrete with glass aggregate: a chemo-physico-mechanical approach.
Kurtis, K., Monteiro, P., Brown, J. and Meyer-Ilse, W. (1998). Imaging of ASR gel by soft X-ray microscopy. Cement and Concrete Research **28**(3): 411-421.
Ling, T.-C. and Poon, C.-S. (2012a). Development of a method for recycling of CRT funnel glass. Environmental technology **33**(22): 2531-2537.
Ling, T.-C. and Poon, C.-S. (2012b). A comparative study on the feasible use of recycled beverage and CRT funnel glass as fine aggregate in cement mortar. Journal of Cleaner Production **29**: 46-52.
Ling, T.-C. and Poon, C.-S. (2014a). Use of CRT funnel glass in concrete blocks prepared with different aggregate-to-cement ratios. Green Materials **2**(1): 43-51.
Ling, T.-C. and Poon, C.-S. (2014b). Feasible use of large volumes of GGBS in 100% recycled glass architectural mortar. Cement and Concrete Composites **53**: 350-356.
Ling, T.-C., Poon, C.-S., Lam, W.-S., Chan, T.-P. and Fung, K. K.-L. (2013). X-ray radiation shielding properties of cement mortars prepared with different types of aggregates. Materials and Structures **46**(7): 1133-1141.
Maraghechi, H., Fischer, G. and Rajabipour, F. (2012). The role of residual cracks on alkali silica reactivity of recycled glass aggregates. Cement and Concrete Composites **34**(1): 41-47.
Maraghechi, H., Rajabipour, F., Pantano, C. G. and Burgos, W. D. (2016). Effect of calcium on dissolution and precipitation reactions of amorphous silica at high alkalinity. Cement and Concrete Research **87**: 1-13.
Marinoni, N., Voltolini, M., Broekmans, M. A., Mancini, L., Monteiro, P. J., Rotiroti, N., Ferrari, E. and Bernasconi, A. (2015). A combined synchrotron radiation micro computed tomography and micro X-ray diffraction study on deleterious alkali-silica reaction. Journal of Materials Science **50**(24): 7985-7997.
Marinoni, N., Voltolini, M., Mancini, L., Vignola, P., Pagani, A. and Pavese, A. (2009). An investigation of mortars affected by alkali-silica reaction by X-ray synchrotron microtomography: a preliminary study. Journal of Materials Science **44**(21): 5815-5823.
Munekuni, S., Dohguchi, N., Nishikawa, H., Ohki, Y., Nagasawa, K. and Hama, Y. (1991). Si—O—Si strained bond and paramagnetic defect centers induced by mechanical fracturing in amorphous SiO2. Journal of Applied Physics **70**(9): 5054-5062.
Neville, A. M. (1995). Properties of concrete.
Nie, Q., Zhou, C., Li, H., Shu, X., Gong, H. and Huang, B. (2015). Numerical simulation of fly ash concrete under sulfate attack. Construction and Building Materials **84**: 261-268.
Nie, Q., Zhou, C., Shu, X., He, Q. and Huang, B. (2014). Chemical, mechanical, and durability properties of concrete with local mineral admixtures under sulfate environment in Northwest China. Materials **7**(5): 3772-3785.
Olafsson, H. (1986). The effect of relative humidity and temperature on alkali expansion of mortar bars. Proc., 7th Int. Conf. on Alkali Aggregate Reaction in Concrete.
Pacchioni, G. (2000). Ab initio theory of point defects in oxide materials: structure, properties, chemical reactivity. Solid State Sciences **2**(2): 161-179.
Paris, J. M., Roessler, J. G., Ferraro, C. C., DeFord, H. D. and Townsend, T. G. (2016). A review of waste products utilized as supplements to Portland cement in concrete. Journal of Cleaner Production **121**: 1-18.
Peterson, K., Carlson, J., Sutter, L. and Van Dam, T. (2009). Methods for threshold optimization for images collected from contrast enhanced concrete surfaces for air-void system characterization. Materials Characterization **60**(7): 710-715.
Peterson, K., Gress, D., Van Dam, T. and Sutter, L. (2006). Crystallized alkali-silica gel in concrete from the late 1890s. Cement and Concrete Research **36**(8): 1523-1532.

Radtsig, V. (1995). Reactive intermediates on the surface of solids (Si02 and Ge02): A review of studies and prospects for their development. Chem. Phys. Reports **14**: 1206-1245.
Rajabipour, F., Maraghechi, H. and Fischer, G. (2010). Investigating the alkali-silica reaction of recycled glass aggregates in concrete materials. Journal of materials in civil engineering **22**(12): 1201-1208.
Saint-Pierre, F., Rivard, P. and Ballivy, G. (2007). Measurement of alkali–silica reaction progression by ultrasonic waves attenuation. Cement and Concrete Research **37**(6): 948-956.
Sanchez, L., Fournier, B., Jolin, M. and Bastien, J. (2014). Evaluation of the stiffness damage test (SDT) as a tool for assessing damage in concrete due to ASR: Test loading and output responses for concretes incorporating fine or coarse reactive aggregates. Cement and Concrete Research **56**: 213-229.
Schwarz, N., Cam, H. and Neithalath, N. (2008). Influence of a fine glass powder on the durability characteristics of concrete and its comparison to fly ash. Cement and Concrete Composites **30**(6): 486-496.
Shayan, A. and Xu, A. (2004). Value-added utilisation of waste glass in concrete. Cement and Concrete Research **34**(1): 81-89.
Shi, C. (2009). Corrosion of glasses and expansion mechanism of concrete containing waste glasses as aggregates. Journal of materials in civil engineering **21**(10): 529-534.
Shi, C. and Zheng, K. (2007). A review on the use of waste glasses in the production of cement and concrete. Resources, Conservation and Recycling **52**(2): 234-247.
Stanton, T. E. (1940). Influence of cement and aggregate on concrete expansion. Engineering News-Record.
Šťastná, A., Šachlová, Š., Pertold, Z., Přikryl, R. and Leichmann, J. (2012). Cathodoluminescence microscopy and petrographic image analysis of aggregates in concrete pavements affected by alkali–silica reaction. Materials Characterization **65**: 115-125.
Sun, X., Guo, S., Dai, Q. and Xiao, X. (2017). Microstructure characterization of alkali-glass particle and alkali-glass powder reacted gels with neutron scattering and imaging techniques. Materials Characterization **131**: 98-107.
Sutter, L. L., Vruno, D. M., Anzalone, G. C. and Dong, J. (2014). Laboratory Study for Comparison of Class C Versus Class F Fly Ash for Concrete Pavement. Michigan Technological University.
Taylor, H., Famy, C. and Scrivener, K. (2001). Delayed ettringite formation. Cement and Concrete Research **31**(5): 683-693.
Van Stappen, J., Bultreys, T., Gilabert, F. A., Hillewaere, X. K., Gómez, D. G., Van Tittelboom, K., Dhaene, J., De Belie, N., Van Paepegem, W. and Du Prez, F. E. (2016). The microstructure of capsule containing self-healing materials: A micro-computed tomography study. Materials Characterization **119**: 99-109.
Vayghan, A. G., Rajabipour, F. and Rosenberger, J. L. (2016). Composition–rheology relationships in alkali–silica reaction gels and the impact on the gel's deleterious behavior. Cement and Concrete Research **83**: 45-56.
Vitro Minerals Company. (2016). "http://www.vitrominerals.com/."
Vitro Minerals Company (2016) "The Technical Note of CoreBlast Media-Recycled Glass Abrasive."
Wan, K. and Xue, X. (2013). In situ compressive damage of cement paste characterized by lab source X-ray computer tomography. Materials Characterization **82**: 32-40.
Yu, R., van Onna, D., Spiesz, P., Yu, Q. and Brouwers, H. (2016). Development of ultra-lightweight fibre reinforced concrete applying expanded waste glass. Journal of Cleaner Production **112**: 690-701.
Zeidan, M. and Said, A. M. (2017). Effect of colloidal nano-silica on alkali–silica mitigation. Journal of Sustainable Cement-Based Materials **6**(2): 126-138.
Zheng, K. (2016). Pozzolanic reaction of glass powder and its role in controlling alkali–silica reaction. Cement and Concrete Composites **67**: 30-38.

549 **Figure Captions:**

550 Fig.1. a) The length change test results of the Type 1, 2, 3 and 4 Samples up to 14 day age; b) The length
551 change test results of the Type 1, 6 and 7 samples up to 28 day age.

552 Fig.2. Demonstration of mortar sample dyeing process with fluorescent epoxy. a) The basic setup of the
553 IU30 Vacuum Impregnation Unit; b) The samples dyed with fluorescent epoxy.

554 Fig.3. Demonstration of ASR damage inside Type 1 samples. a) and d): Demonstration of cracks inside
555 the reactive glass aggregate; b) and e): Indication of the cracks along the aggregate boundary; c) and f):
556 Depiction of ASR damage in the area close to air voids.

557 Fig.4. Demonstration of the reduction effect of added SCMs on ASR damage. a), b), c) and d)
558 Demonstration of reduced ASR damage in Type 2, 3, 4 and 5 Samples.

559 Fig.5. Demonstration of the ASR damage of mortar samples with SCMs. a), b), c) and d) Demonstration
560 of the ASR damage in Type 2, 3, 4 and 5 Samples.

561 Fig.6. Demonstration ASR damage in type 1 sample using ESEM. a): Demonstration of the cracks existed
562 in both aggregate and cement paste induced by the ASR gel; b) The magnification of the Area A in Fig. 6
563 a) for the better demonstration of cracks in cement paste; c) The element mapping analysis results based
564 on EDS within the area shown in Fig. 6 b).

565 Figure 7. Demonstration of the ASR damage in the sample with added glass powder a): Demonstration of
566 the ASR damage features in type 3 sample; b) Magnification of the Area A shown in Fig. 7 a) for the
567 demonstration of generated ASR gel.

568 Fig.8. Demonstration of the ASR damage in the sample with added glass powder a): Demonstration of the
569 ASR damage features in type 4 sample; b) Magnification of the Area A shown in Fig. 8 a) for the
570 demonstration of cracks inside glass aggregate.

571 Fig.9. Demonstration of the ASR damage in the sample with added fly ash a) and b): Demonstration of
572 the ASR damage features in type 5 sample.

573 Fig.10. The dynamic development of ASR deterioration in aggregate. A) The initial scanning at 0 reaction
574 hours; B) The scanning at 12 reaction hours; C) The scanning at 36 reaction hours; D) The final scanning
575 at 63 reaction hours.

576 Fig.11. Demonstration of the developed ASR damage from the area with initial defects. a) and c) The
577 original aggregate morphology at 0 hour reaction age; b) and d) The aggregate morphology after ASR
578 damage at the 63 hours reaction age.

579 Fig.12. Indication of cracks developed from sharp corner. a) Glass particle with sharp corner and initial
580 defect at 0 hour reaction age and b) Developed cracks in glass particle at 63 hours reaction age.

581 Fig.13. ASR damage feature for the static examined samples (7 day age). a) The examination results of
582 controlled sample. b) The examination results of the sample with added fly ash; c) The examination
583 results of the sample with added glass powder.

584 **Table 1**

585 Mix design of the mortar samples containing reactive glass aggregate

	Cement	SCMs	Glass Aggregate	Water
Type 1 (control type)	440 g	-	990 g	206.8 g
Type 2	374 g	66 g (LA 300 Type)	990 g	206.8 g
Type 3	374 g	66 g (CS 325 Type)	990 g	206.8 g
Type 4	374 g	66 g (LA 800 Type)	990 g	206.8 g
Type 5	374 g	66 g (Class F fly ash)	990 g	206.8 g
Type 6	308 g	132 g (LA 300 Type)	990 g	206.8 g
Type 7	308 g	132 g (LA 800 Type)	990 g	206.8 g

586

587

588 **Table 2**
589 Details of chemical composition and mesh size of SCMs

		CS 325	LA 300	LA 800	Fly Ash (Sutter et al., 2014)
Chemical Composition (mass percentage)	SiO2	50-80%	50-55%	50-55%	47.3%
	Al2O3	1-10%	14-20%	14-20%	23.4%
	CaO	5-15%	20-25%	20-25%	3.8%
	Na2O+K2O	2-16%	8-14%	8-14%	2.4%
Particle Size (μm)	D50 median size	50	60	20	-
	D98 top size	10-12	10-12	6-7	45

590

591

592 **Table 3**

593 The chemical composition analysis results of the type 1 sample

	O (Wt %)	Si (Wt %)	Na (Wt %)	K (Wt %)	Ca (Wt %)	Al (Wt %)	Mg (Wt %)	Alkali:Si Molar ratio	Ca:Si Molar Ratio	Al:Si Molar Ratio
Site 1	52.0	23.5	8.0	0.2	13.6	1.2	1.5	0.42	0.40	0.053
Site 2	50.6	24.4	6.1	0.2	17.0	1.3	0.4	0.31	0.49	0.055
Site 3	46.9	22.8	11.6	0.4	17.3	0.9	0.1	0.63	0.53	0.041

594

595

596 **Table 4**

597 The chemical composition analysis results of the type 3 sample

	O (Wt %)	Si (Wt %)	Na (Wt %)	K (Wt %)	Ca (Wt %)	Al (Wt %)	Mg (Wt %)	Alkali:Si Molar ratio	Ca:Si Molar ratio	Al:Si Molar ratio
Site S1	51.63	25.94	9.41	1.23	10.53	0.81	0.45	0.48	0.28	0.032
Site S2	50.54	26.51	10.11	1.23	10.32	0.85	0.44	0.50	0.27	0.033

598

599

600 **Table 5**

601 The chemical composition analysis results of the type 4 sample

	O (Wt %)	Si (Wt %)	Na (Wt %)	K (Wt %)	Ca (Wt %)	Al (Wt %)	Mg (Wt %)	Alkali:Si Molar ratio	Ca:Si Molar ratio	Al:Si Molar ratio
Site S1	48.8	28.1	10.7	1.0	10.8	0.6	-	0.49	0.27	0.022
Site S2	46.8	29.5	10.4	1.1	11.6	0.6	-	0.46	0.28	0.021
Site S3	48.4	29.3	9.4	0.9	11.4	0.6	-	0.41	0.27	0.021

602

603

604 **Table 6**

605 The chemical composition analysis results of the Type 5 sample

	O (Wt %)	Si (Wt %)	Na (Wt %)	K (Wt %)	Ca (Wt %)	Al (Wt %)	Mg (Wt %)	Alkali:Si Molar ratio	Ca:Si Molar ratio	Al:Si Molar ratio
Site S1	48.3	29.2	7.3	2.6	11.0	0.9	0.7	0.37	0.26	0.032
Site S2	47.6	29.4	7.5	2.5	11.4	0.8	0.8	0.37	0.27	0.029

606

607

608

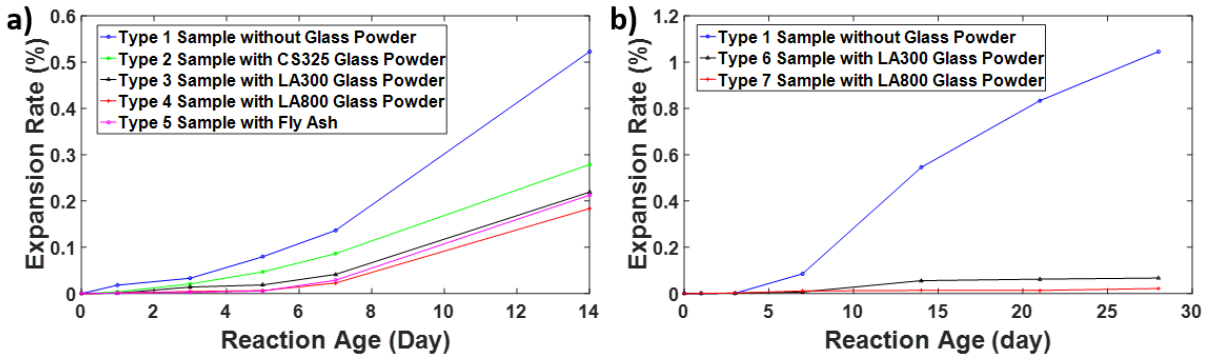

609 Fig.1. a) The length change test results of the Type 1, 2, 3 and 4 Samples up to 14 day age; b) The length
610 change test results of the Type 1, 6 and 7 samples up to 28 day age.

611

612

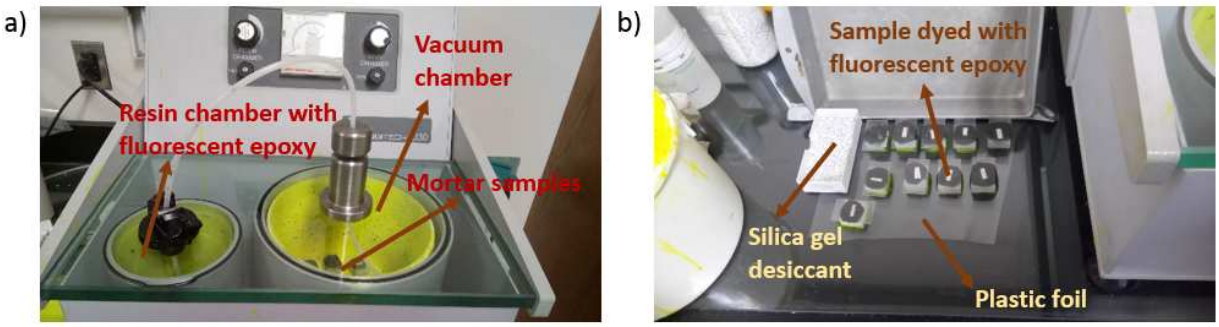

613 Fig.2. Demonstration of mortar sample dyeing process with fluorescent epoxy. a) The basic setup of the
614 IU30 Vacuum Impregnation Unit; b) The samples dyed with fluorescent epoxy.

615

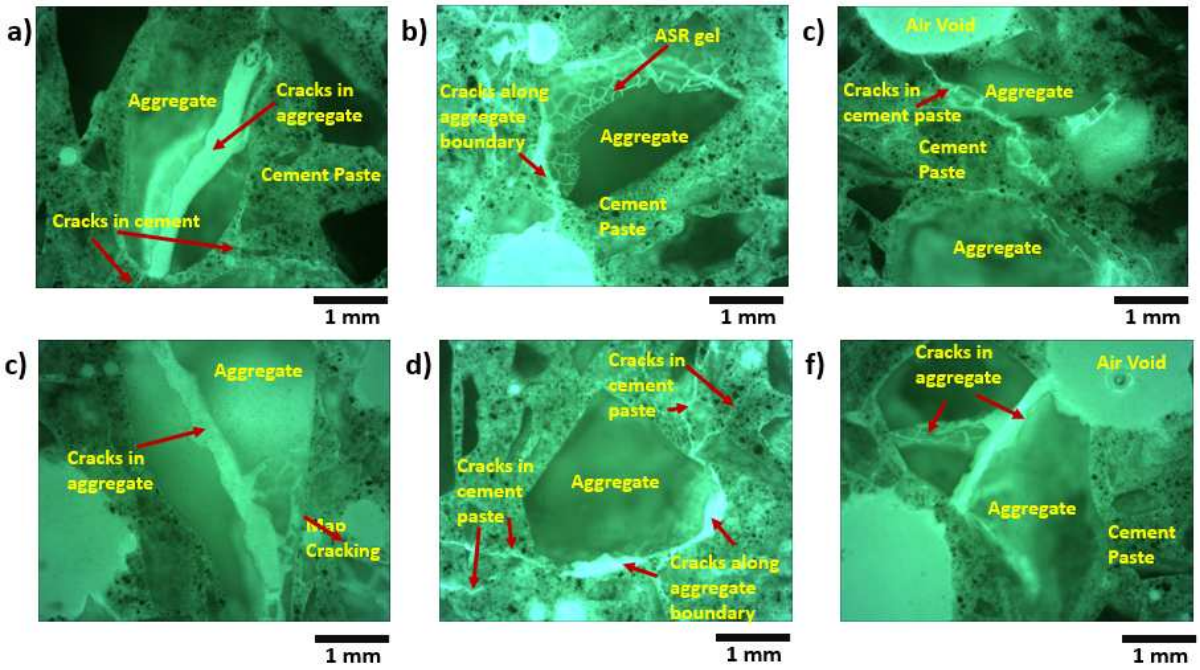

616

617 Fig.3. Demonstration of ASR damage inside Type 1 samples. a) and d): Demonstration of cracks inside
618 the reactive glass aggregate; b) and e): Indication of the cracks along the aggregate boundary; c) and f):
619 Depiction of ASR damage in the area close to air voids.

620

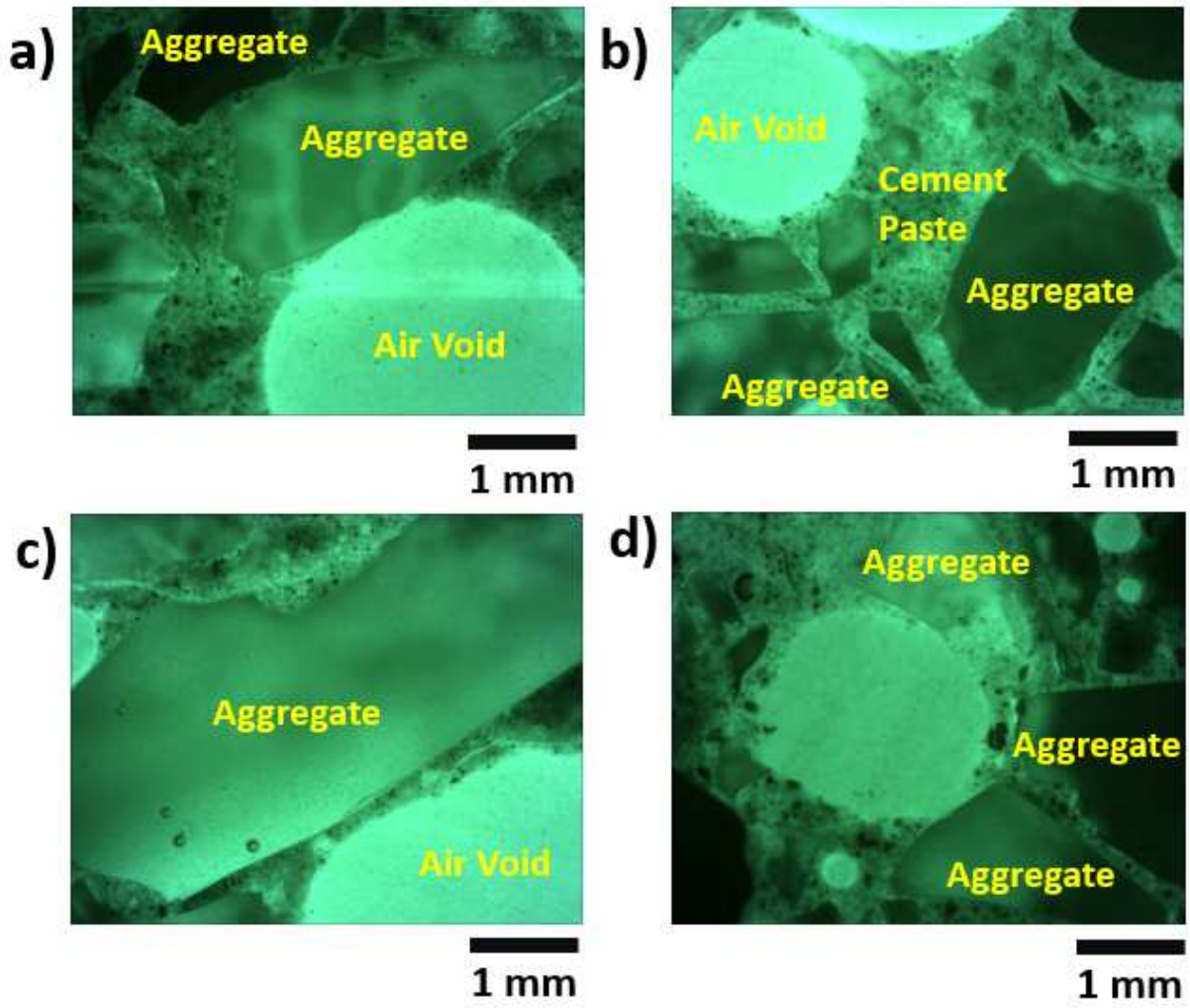

621

622 Fig.4. Demonstration of the reduction effect of added SCMs on ASR damage. a), b), c) and d)
623 Demonstration of reduced ASR damage in Type 2, 3, 4 and 5 Samples.

624

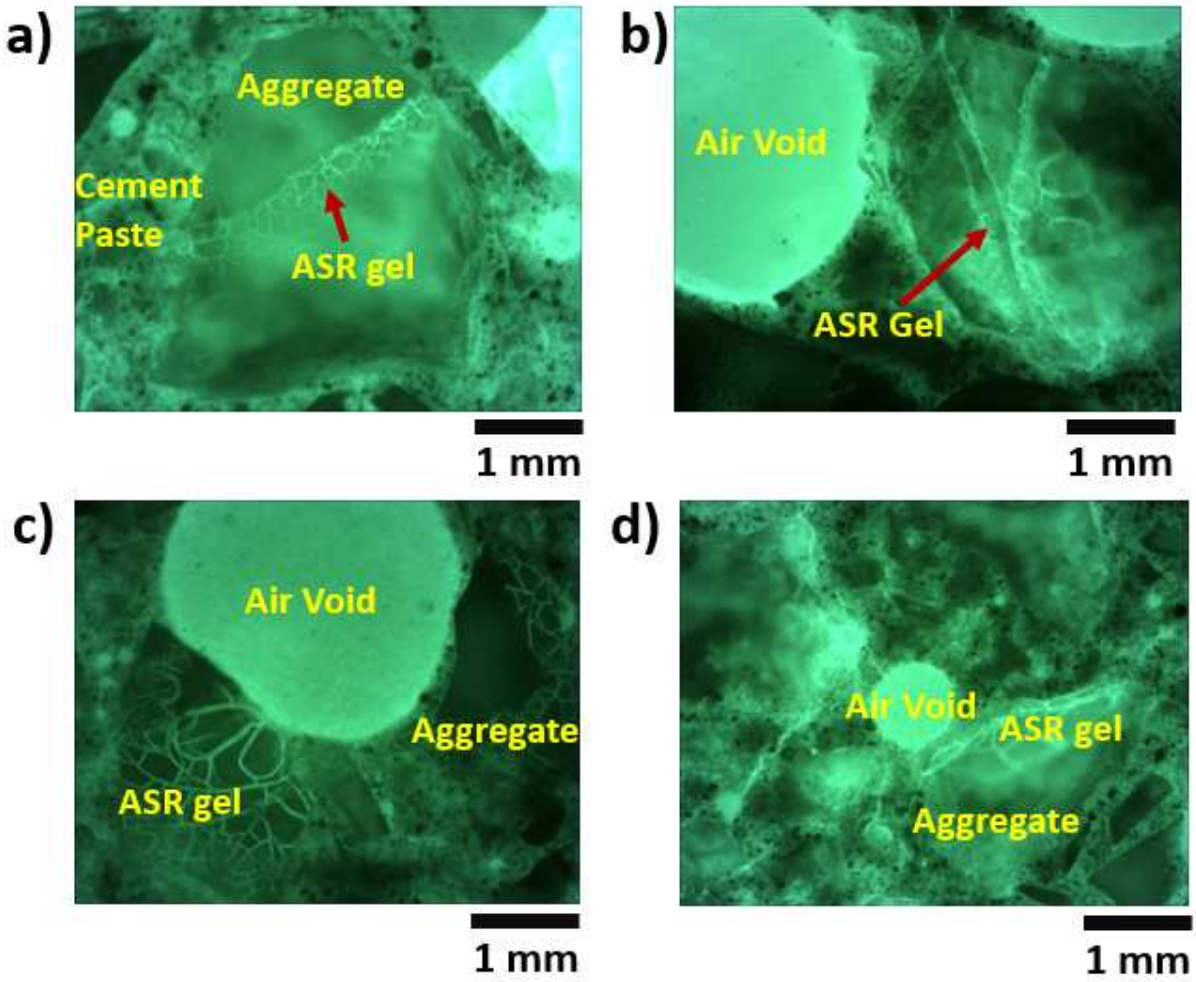

625

626 Fig.5. Demonstration of the ASR damage of mortar samples with SCMs. a), b), c) and d) Demonstration
627 of the ASR damage in Type 2, 3, 4 and 5 Samples.

628

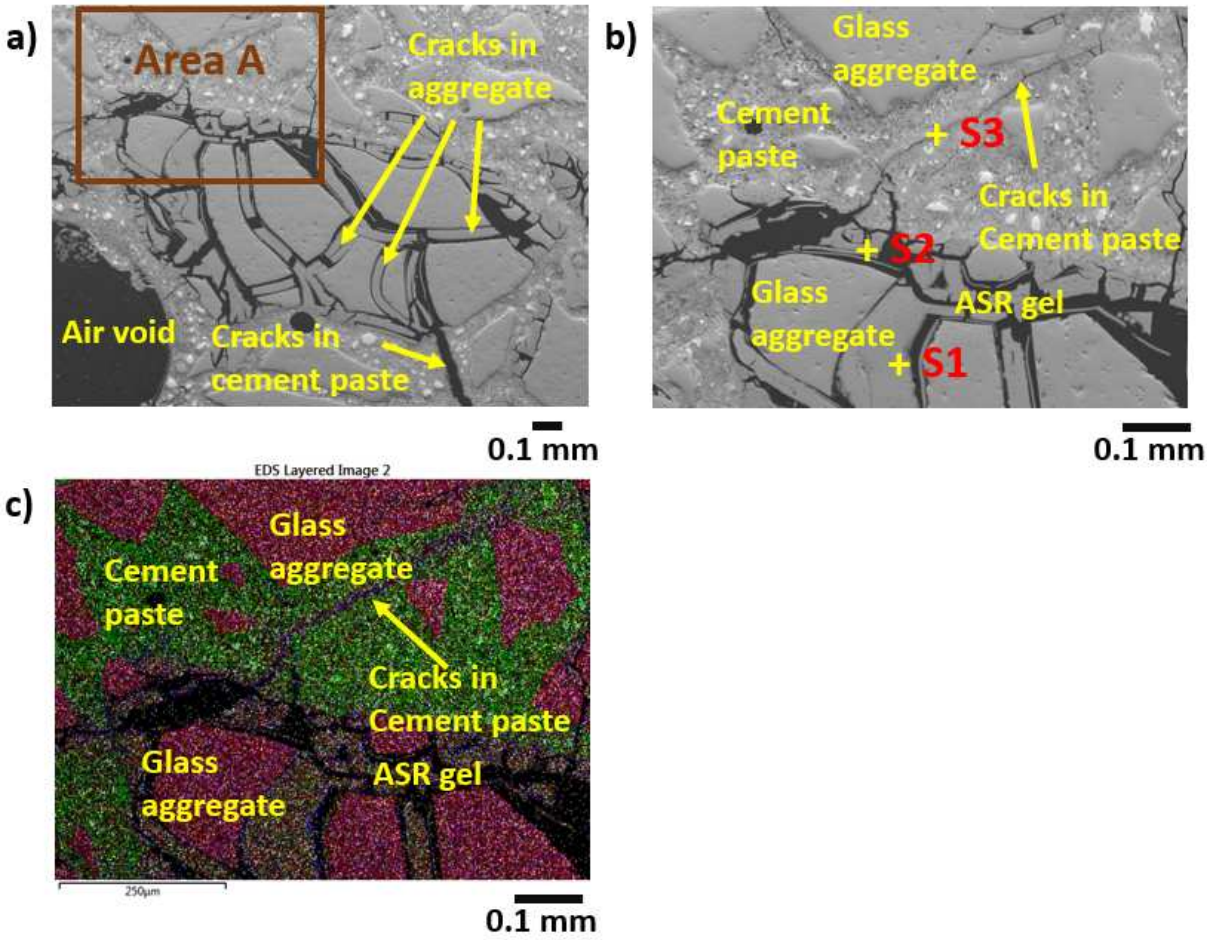

629

630 Fig.6. Demonstration ASR damage in type 1 sample using ESEM. a): Demonstration of the cracks existed
631 in both aggregate and cement paste induced by the ASR gel; b) The magnification of the Area A in Fig. 6
632 a) for the better demonstration of cracks in cement paste; c) The element mapping analysis results based
633 on EDS within the area shown in Fig. 6 b).

634

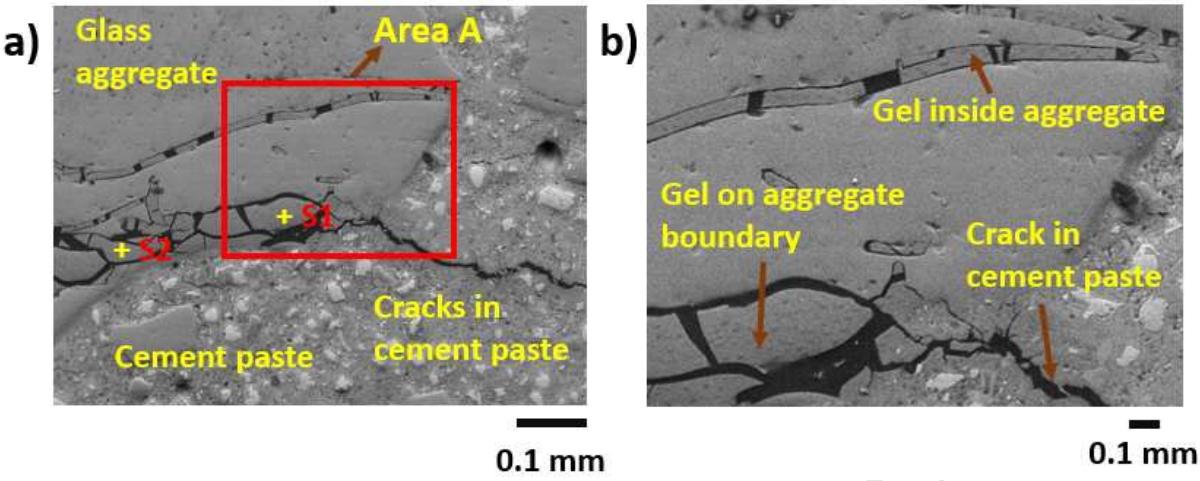

635

636 Figure 7. Demonstration of the ASR damage in the sample with added glass powder a): Demonstration of
637 the ASR damage features in type 3 sample; b) Magnification of the Area A shown in Fig. 7 a) for the
638 demonstration of generated ASR gel.

639

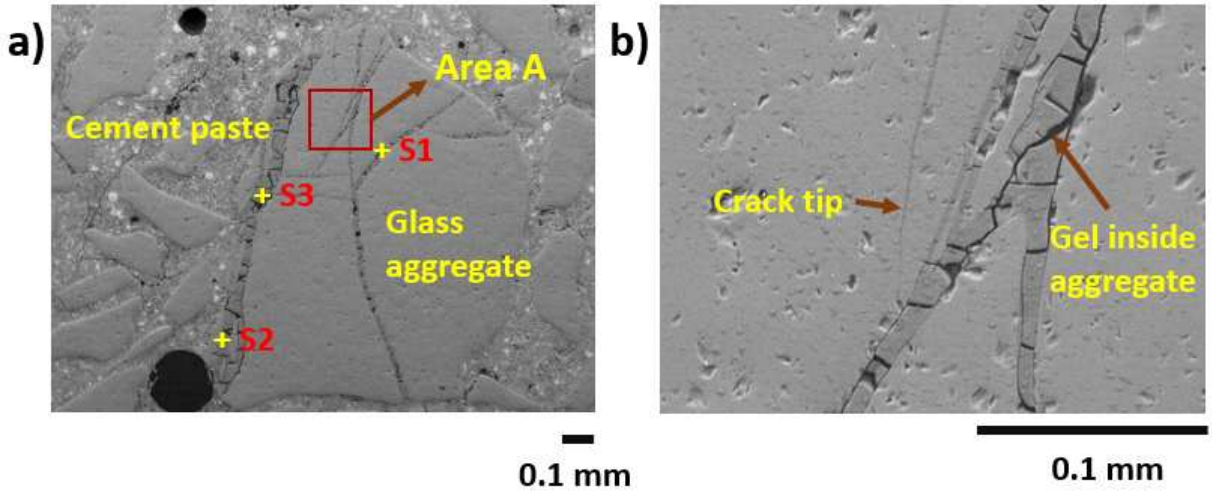

Fig.8. Demonstration of the ASR damage in the sample with added glass powder a): Demonstration of the ASR damage features in type 4 sample; b) Magnification of the Area A shown in Fig. 8 a) for the demonstration of cracks inside glass aggregate.

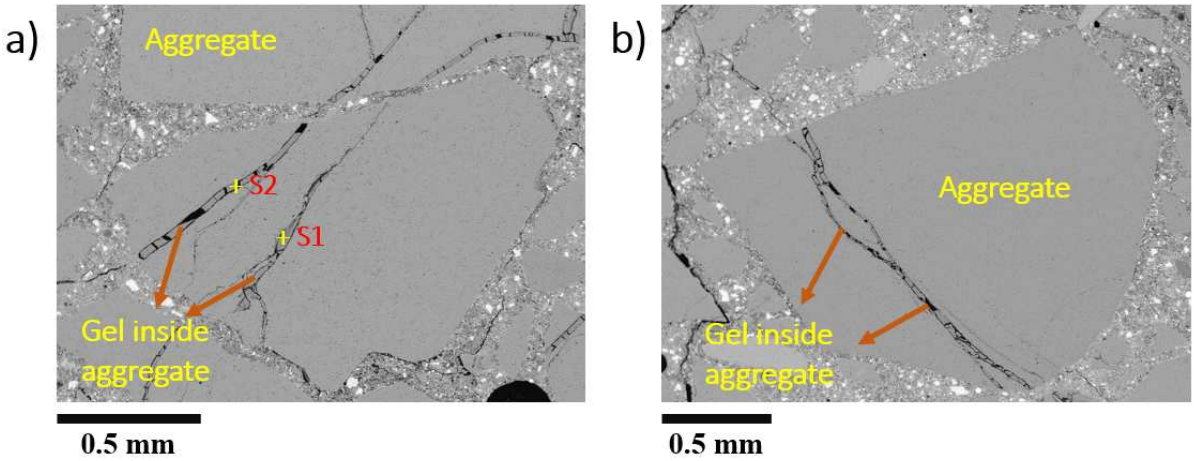

645

646 Fig.9. Demonstration of the ASR damage in the sample with added fly ash a) and b): Demonstration of
647 the ASR damage features in type 5 sample.

648

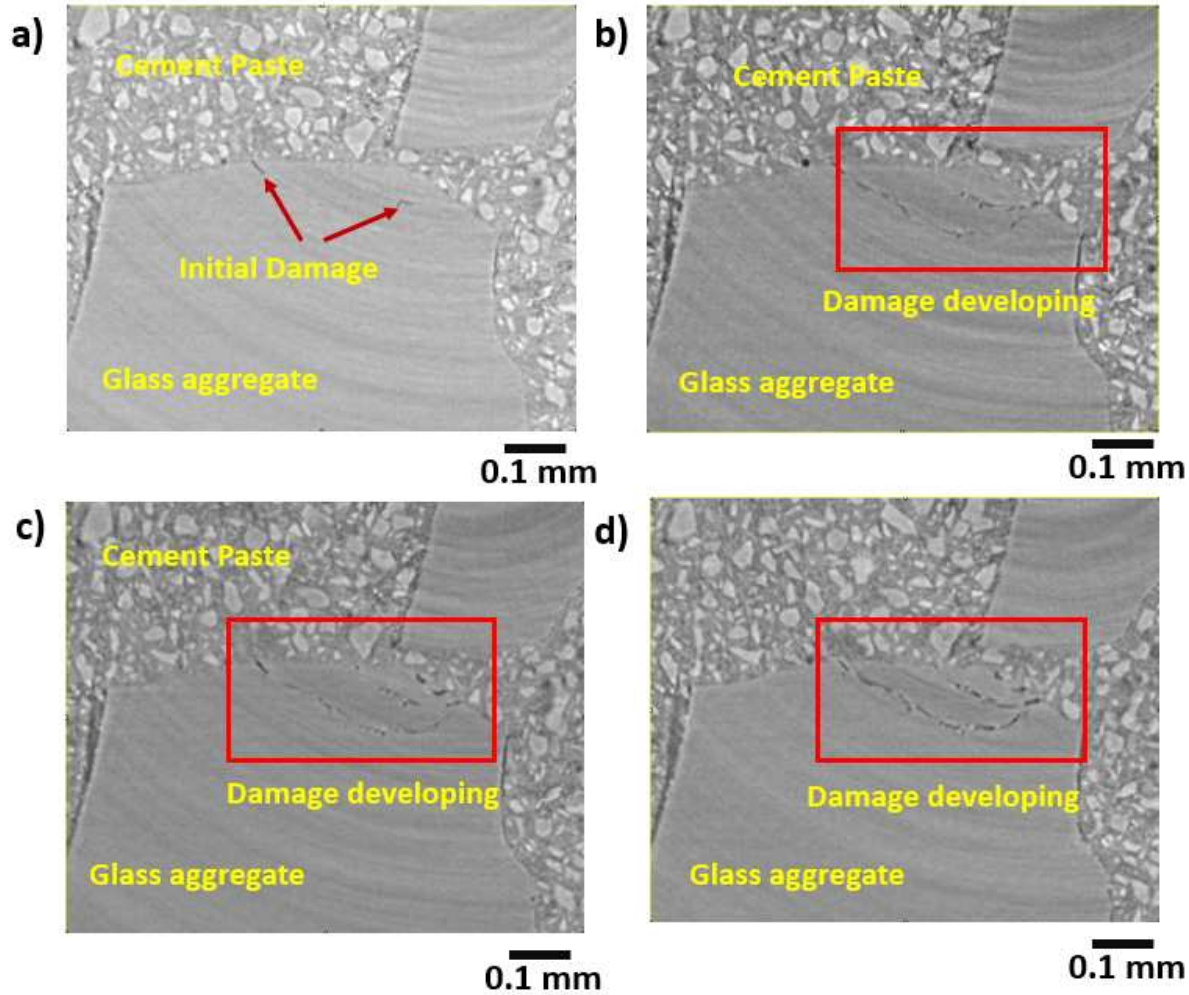

649

650 Fig.10. The dynamic development of ASR deterioration in aggregate. A) The initial scanning at 0 reaction
651 hours; B) The scanning at 12 reaction hours; C) The scanning at 36 reaction hours; D) The final scanning
652 at 63 reaction hours.

653

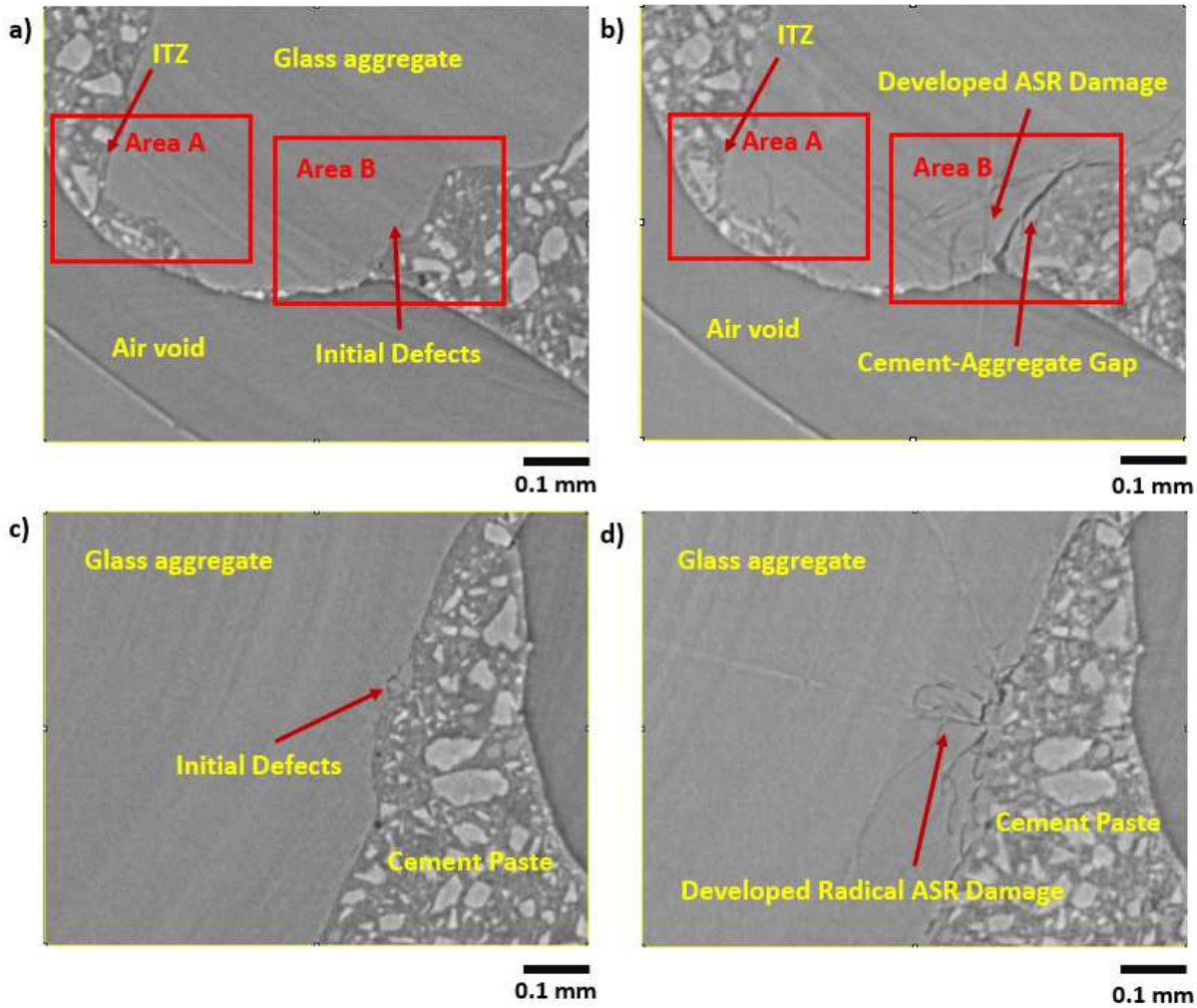

654

655 Fig.11. Demonstration of the developed ASR damage from the area with initial defects. a) and c) The
656 original aggregate morphology at 0 hour reaction age; b) and d) The aggregate morphology after ASR
657 damage at the 63 hours reaction age.

658

659

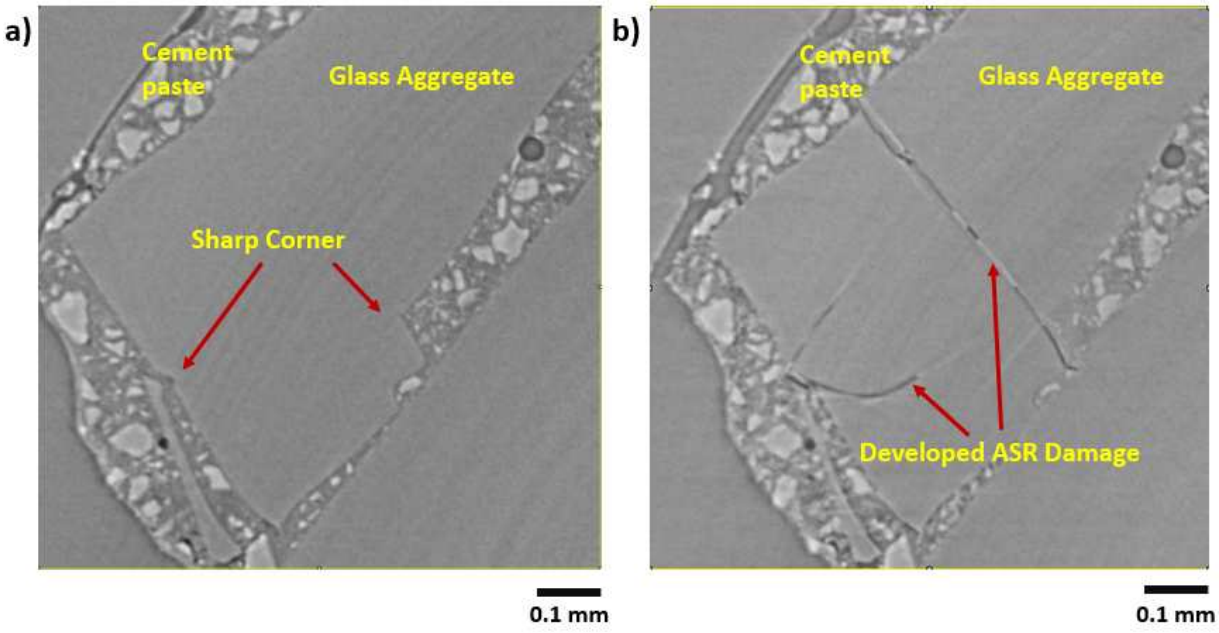

660

661 Fig.12. Indication of cracks developed from sharp corner. a) Glass particle with sharp corner and initial
662 defect at 0 hour reaction age and b) Developed cracks in glass particle at 63 hours reaction age.

663

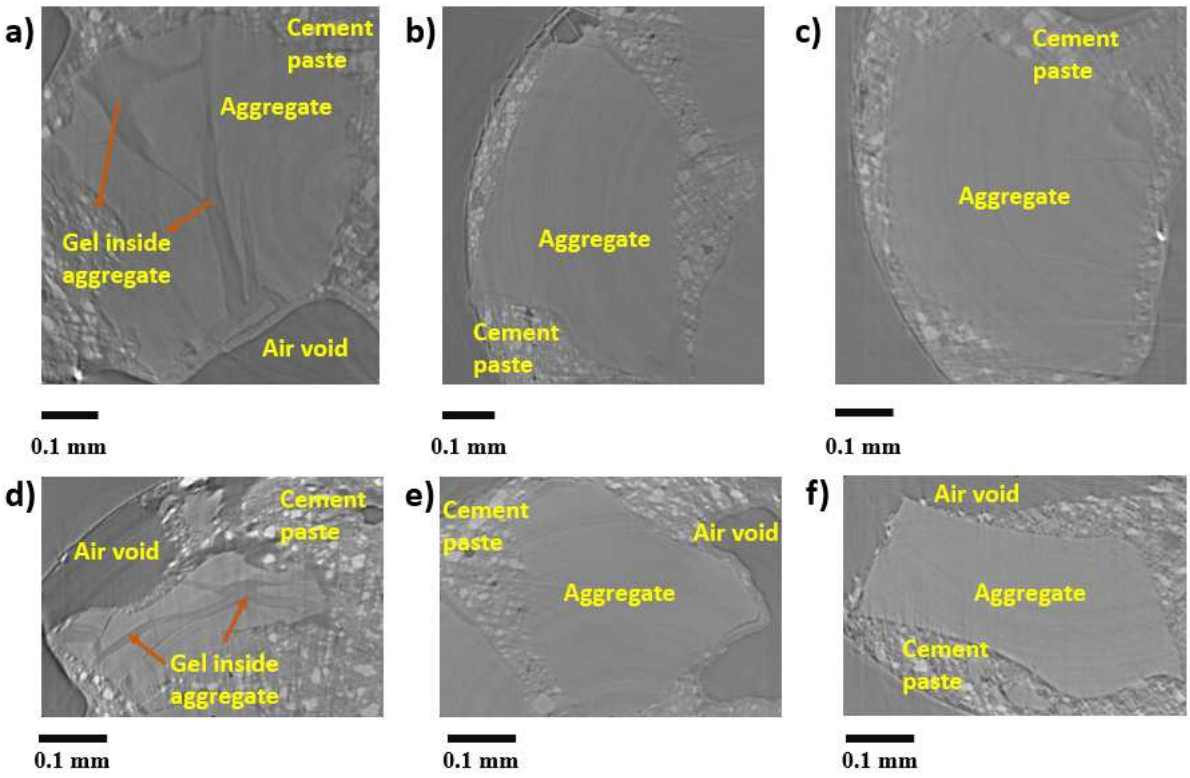

Fig.13. ASR damage feature for the static examined samples (7 day age). a) and d) The examination results of controlled sample. b) and e) The examination results of the sample with added fly ash; c) and f) The examination results of the sample with added glass powder.